

Accepted for publication in ApJ

# Velocity Distributions from Nonextensive Thermodynamics

Eric I. Barnes

*Department of Physics, University of Wisconsin — La Crosse, La Crosse, WI 54601*

`barnes.eric@uwlax.edu`

Liliya L. R. Williams

*Department of Astronomy, University of Minnesota, Minneapolis, MN 55455*

`llrw@astro.umn.edu`

Arif Babul<sup>1</sup>

*Department of Physics & Astronomy, University of Victoria, BC, Canada*

`babul@uvic.ca`

Julianne J. Dalcanton<sup>2</sup>

*Department of Astronomy, University of Washington, Box 351580, Seattle, WA 98195*

`jd@astro.washington.edu`

## ABSTRACT

There is no accepted mechanism that explains the equilibrium structures that form in collisionless cosmological N-body simulations. Recent work has identified nonextensive thermodynamics as an innovative approach to the problem. The distribution function that results from adopting this framework has the same form as for polytropes, but the polytropic index is now related to the degree of nonextensiveness. In particular, the nonextensive approach can mimic the equilibrium structure of dark matter density profiles found in simulations. We extend the investigation of this approach to the velocity structures expected from

---

<sup>1</sup>Leverhulme Visiting Professor, Universities of Oxford and Durham

<sup>2</sup>Alfred P. Sloan Foundation Fellow

nonextensive thermodynamics. We find that the nonextensive and simulated N-body  $v_{\text{rms}}$  distributions do not match one another. The nonextensive  $v_{\text{rms}}$  profile is either monotonically decreasing or displays little radial variation, each of which disagrees with the  $v_{\text{rms}}$  distributions seen in simulations. We conclude that the currently discussed nonextensive models require further modifications in order to corroborate dark matter halo simulations.

*Subject headings:* dark matter — galaxies:structure — galaxies:kinematics and dynamics

## 1. Introduction

Simulations of structure formation have become well-refined and sophisticated over the past few decades. Typically, N-body simulations follow collisionless particles that represent dark matter and hierarchically form gravitationally bound structures. These structures have several “universal” characteristics, among them their self-similar density profiles (*e.g.*, Navarro *et al.* 1996; Moore *et al.* 1998; Power *et al.* 2003). However, as of yet there is no accepted physical mechanism for explaining these shared properties, although there is no lack of hypotheses (*e.g.*, Lokas 2000; Nusser 2001; Barnes *et al.* 2005; Lu *et al.* 2006). This work further examines the recently advanced suggestion that nonextensive thermodynamics can be used to determine the equilibria (Hansen *et al.* 2005; Leubner 2005; Hansen & Moore 2006; Kronberger, Leubner, van Kampen 2006). For simplicity, we deal only with spherically symmetric systems in this work.

### 1.1. Nonextensive Thermodynamics

The lack of short-range forces in self-gravitating, collisionless systems throws the adoption of standard thermodynamics into question. Instead, Tsallis (1988) has proposed a generalized themodynamical approach for such systems based on the nonextensiveness of entropy; *i.e.*, the entropy of a composite system is not simply the sum of the subsystems’ entropies. In particular, the entropy of a composite system is given by,

$$S_{A+B} = S_A + S_B + (1 - q)S_A S_B, \quad (1)$$

where  $S$  is the entropy,  $A$  and  $B$  refer to subsystems, and  $q$  is a parameter that describes the degree of nonextensiveness. When  $q = 1$  the situation is extensive and corresponds

to standard thermodynamics. Nonextensive thermodynamics (sometimes referred to as  $q$ -statistics) has been designed to describe systems with long dynamical memories, as in self-gravitating collisionless objects. Although other applications have been discussed by Tsallis (1999), specific applications of nonextensive thermodynamics to astrophysical situations have been discussed by Plastino & Plastino (1993); Aly (1993); Hansen *et al.* (2005); Leubner (2005), and most recently by Kronberger, Leubner, van Kampen (2006, hereafter KKK). One of the more interesting results of the nonextensive approach is that the associated distribution function has the same form as for a polytrope (Plastino & Plastino 1993). In this case, the analogue to the polytropic index is related to the  $q$  value (see § 2.1). Hansen & Moore (2006) appeal to nonextensive thermodynamics to interpret the correlation between density profile slope and velocity anisotropy observed in N-body simulations. KKK have found that the density profiles corresponding to nonextensive distribution functions can be found to match those of virialized dark matter halos formed in cosmological simulations. These studies have demonstrated that nonextensive thermodynamics is an attractive option for theoretically grounding the behavior seen in computer simulations. After a brief synopsis of relevant halo properties, we will discuss our findings that nonextensive thermodynamics, as it currently stands, does not provide such a basis.

## 1.2. Overview of Simulated Dark Matter Halo Properties

The virialized structures (halos) that are formed in cosmological N-body simulations have several properties that appear to be “universal”. Density profiles have nonpower law shapes where a scalelength divides a steeply declining outer region from a less steeply declining inner cusp. Most previous works investigating halo formation focus on explaining this kind of density profile. However, the velocity structures of the halos are also important. Like the density profiles, N-body halo velocity dispersion distributions  $v_{\text{rms}}(r)$  have nonpower law shapes which peak near the density scalelength. The relevance of  $v_{\text{rms}}$  can be illustrated by the quantity  $\rho/v_{\text{rms}}^3$  which is reminiscent of and shares the dimensionality of the phase space density. As first noted in Taylor & Navarro (2001), this quantity follows a power law distribution with radius  $\rho/v_{\text{rms}}^3 \propto r^{-\alpha}$ , where  $\alpha$  is a constant that depends on the particular density profile. This behavior appears to be linked to the physics of collisionless collapse, given that the same power laws result from independent semi-analytical halo formation models, as shown by Austin *et al.* (2005). The velocity structures of dark matter halos therefore provide additional leverage for understanding the physical mechanisms that drive equilibrium halo formation.

## 2. Nonextensive Isotropic Equilibria

KLK demonstrate that the equilibrium density profiles of sufficiently nonextensive systems with velocity isotropy describe the results of N-body simulations well (see Figure 2 of KLK). Their work maintains a constant degree of nonextensiveness  $q$ . To maintain continuity with KLK, we will adopt their variable  $\kappa = 1/(1 - q)$  as the measure of nonextensiveness. We first investigate the predicted velocity dispersion for these models, and then we proceed to allow  $\kappa(r)$  to vary.

### 2.1. Constant $\kappa$

Starting with the nonextensive definition of entropy (Tsallis 1988),

$$S_\kappa = k_B \kappa \left( \sum_i p_i^{1-1/\kappa} - 1 \right), \quad (2)$$

where  $k_B$  is Boltzmann’s constant and the sum is over all accessible states (each with probability  $p_i$ ), one can extremize  $S_\kappa$  under the constraints of constant total mass and energy to find the distribution function, as in Plastino & Plastino (1993). Silva, Plastino, & Lima (1998) find that the same nonextensive velocity distribution functions can be found using a variation on Maxwell’s derivation of the standard distribution functions, independent of any assumptions about energy. As Silva, Plastino, & Lima (1998) make clear, the nonextensive approach demands velocity isotropy.

Assuming a spherical system and adopting the Poisson equation as the link between density and potential, the nonextensive distribution function is obtained (Plastino & Plastino 1993; Kronberger, Leubner, van Kampen 2006),

$$f^\pm(E_r) = B^\pm \left[ 1 + \frac{E_r}{\kappa \sigma^2} \right]^{-\kappa}, \quad (3)$$

where  $E_r \equiv v^2/2 - \Psi$  is the relative specific energy,  $v^2/2$  is the specific kinetic energy,  $\Psi = -\Phi + \Phi_0$  ( $\Phi$  is the specific potential energy and  $\Phi_0$  is a constant), and  $\sigma$  is an energy normalization constant. The ‘ $\pm$ ’ denotes that  $\kappa$  can be positive or negative and the normalization constant  $B$  reflects that choice. Again, note that this distribution function is exactly that for a polytrope (Plastino & Plastino 1993). The nonextensive thermodynamic framework provides a physical meaning to the polytropic index; it is a measure of nonextensiveness. With this distribution function [which is isotropic since  $f = f(E_r)$ ], it can be shown that the density is,

$$\frac{\rho^\pm}{\rho_0} = \left[ 1 - \frac{\Psi}{\kappa \sigma^2} \right]^{3/2-\kappa} \quad (4)$$

and the rms velocity distribution is given by,

$$\frac{v_{\text{rms}}^{\pm}}{v_0} = \left[ 1 - \frac{\Psi}{\kappa \sigma^2} \right]^{1/2}, \quad (5)$$

where  $v_{\text{rms}} \equiv \langle v^2 \rangle^{1/2}$ . We note that Equation 5 is reminiscent of the expression for the outer halo velocity dispersion given in Equation 3 of Hoesft, Mücke, & Gottlöber (2004). It is straightforward to show that these functions satisfy the Jeans equation for mechanical equilibrium. Equation 4 can be solved for  $\Psi$  and combined with the Poisson equation,

$$\nabla^2 \Psi = -4\pi G \rho \quad (6)$$

to form a second-order differential equation for  $\rho$  that we solve numerically.

We turn our attention here to the velocity profiles given by Equation 4. We will specifically consider profiles with  $\kappa < 0$ , like those discussed in KLK, for reasons discussed at the end of § 2.2. For large values of  $|\kappa|$  (*i.e.*, as a system becomes increasingly extensive),  $v_{\text{rms}}$  approaches a constant as the density profile becomes isothermal, as expected. For more modest values of  $\kappa < 0$ ,  $v_{\text{rms}}$  is always a continuously decreasing function of radius. However, this is not what is seen in the results of cosmological N-body simulations, for which  $v_{\text{rms}}$  has a well defined peak near the scalelength of the halo density profile  $r_0$ .

Another view of this discrepancy is given by the phase-space density-like quantity  $\rho/v_{\text{rms}}^3$ . The solid red lines in Figure 1 represent nonextensive density (panel a), velocity dispersion (panel b), and  $\rho/v_{\text{rms}}^3$  profiles (panel c) using the KLK values  $\kappa = -15$ ,  $\sigma = 0.12$ . Note that the density and  $\rho/v_{\text{rms}}^3$  distributions have been scaled by  $(r/r_0)^{-2}$  to highlight differences from this power law profile. Figure 1 also shows  $\rho$ ,  $v_{\text{rms}}$ , and  $\rho/v_{\text{rms}}^3$  profiles for isotropic Navarro *et al.* (1996, hereafter NFW) (dashed blue lines) and Navarro *et al.* (2004, hereafter N04) (dash-dotted green lines) models for comparison. In the end, although a nonextensive, constant  $\kappa$  density profile can be found to mimic the density profiles found in cosmological simulations, the corresponding velocity structures do not match.

## 2.2. Variable $\kappa$

We now relax the constraint of constant  $\kappa$  and allow for  $\kappa(r)$  distributions. As before, Jeans equilibrium is maintained. Varying  $\kappa$  introduces derivatives of  $\kappa$  to Equation 6, in addition to the derivatives of  $\rho$ , allowing us to choose either: A) a  $\rho$  distribution and solve for  $\kappa(r)$ , or B) a  $\kappa$  distribution and solve for  $\rho(r)$ . We have tested our numerical implementations of these approaches for self-consistency.

Accounting for radial variations of  $\kappa$  is especially pertinent given that it has recently been found that there is a direct connection between  $\kappa$  (or  $q$ ) and the slope of a density profile (Hansen *et al.* 2005). The radial changes in density slope present in dark matter halo models (*e.g.*, density slopes change from -1 to -3 as radius increases in NFW profiles) then demand radial variation of  $\kappa$ .

Following track A discussed above, both NFW and N04 density profiles lead to derived  $\kappa$  distributions that are always negative. While we discuss the N04 profile in detail here, the NFW results are essentially the same. Figure 2 shows the scaled N04 density profile (panel a), three  $\kappa$  profiles (panel b), and the resulting  $v_{\text{rms}}$  distributions (panel c). The solid blue, dashed green, and dash-dotted red lines represent solutions when  $\kappa_{\text{init}} = -5, -15$ , and  $-20$ , respectively. We could not find solutions with positive  $\kappa$  values over any section of the distribution. The resulting  $\kappa$  distributions have roughly sinusoidal shapes superimposed on linear trends which vary with the adopted initial  $\kappa$  value; for  $\kappa_{\text{init}} \gtrsim -17$  the linear trends have negative slopes, for  $\kappa_{\text{init}} \lesssim -17$  the trends are positive. While these profiles are interesting in their own right, the relevance to the current work is that the resulting velocity dispersion profiles in Figure 2c remain monotonically decreasing functions, like the constant  $\kappa$  case (solid line in Figure 1b). We conclude that the nonextensive distribution given in Equation 3 does not reproduce all aspects of N-body simulation results.

As track A fails to produce velocity dispersions similar to those in simulations, we now discuss a  $\kappa$  distribution designed to remedy this problem. We seek a function that is positive (negative) for radii smaller (larger) than  $r_0$ . This should give us a dispersion profile that peaks near  $r_0$ . Since  $\kappa = 0$  leads to infinite entropy, we cannot simply transition from positive to negative values. These arguments have led us to choose the following form,

$$\kappa(r) = -A \coth[s \log(r/r_0)], \quad (7)$$

where  $\kappa \rightarrow A$  as  $\log r/r_0 \rightarrow -\infty$ ,  $\kappa \rightarrow -A$  as  $\log r/r_0 \rightarrow \infty$ , and  $s$  determines the rate of change between  $A$  and the infinite value at  $\log r/r_0 = 0$ . As many functions can be created with similar properties, we discuss this specific form only as an illustrative example.

The  $\kappa$  profile described by Equation 7 is shown in Figure 3a. Where  $\kappa < 0$ , we plot  $-\log|\kappa|$ . A density profile that reasonably approximates those from simulations has the following parameter values;  $A = 25$ ,  $s = 0.5$ , and  $\sigma = 0.12$  (Figure 3b). As in Figure 1, the solid red, dashed blue, and dash-dotted green lines represent solution, NFW, and N04 profiles, respectively. The  $v_{\text{rms}}$  distribution now has the correct qualitative behavior; it is a rising function near the center and decreases with increasing  $r > r_0$  (Figure 3c). However, it does not quantitatively match simulation results. Specifically, the  $v_{\text{rms}}$  profile is too flat. This difference is also apparent when looking at the  $\rho/v_{\text{rms}}^3$  distributions in Figure 3d. The  $\rho/v_{\text{rms}}^3$  profile from the nonextensive approach closely resembles the density, which has a

decidedly nonpower law shape. There simply is not enough variation in the  $v_{\text{rms}}$  distribution to compensate the changes in  $\rho$  and produce a power law. Such discrepancies may reflect the insufficiency of Equation 7; further work may suggest more appropriate  $\kappa(r)$  expressions.

We note that this use of  $\kappa > 0$  for  $\log r/r_0 < 0$  contradicts the arguments made in KLK and Leubner (2005). Leubner (2005) points out that negative  $\kappa$  means: 1) that the entropy of a composite system is less than in the extensive case, and 2) the heat capacity is negative.  $\kappa > 0$  implies a positive heat capacity, indicative of a system in which self-gravity is not important. We do not speculate further on the implications of this interpretation. Positive  $\kappa$  has been adopted simply to get the  $v_{\text{rms}}$  profile to have positive slope at small  $r$  like the simulation results.

### 3. Summary & Conclusions

It has been recently shown that nonextensive thermodynamics can be used to explain the density profiles of collisionless dark matter halos formed in cosmological N-body simulations (Kronberger, Leubner, van Kampen 2006, KLK). While this is an important step forward in understanding the physics governing collisionless equilibria, N-body simulations also find universal links between density and velocity distributions, such as the power law behavior of  $\rho/v_{\text{rms}}^3$  (*e.g.*, Taylor & Navarro 2001). Can nonextensive thermodynamics correctly predict the velocity behavior of systems formed in cosmological simulations?

We find that a constant nonextensiveness parameter  $\kappa$  (as in KLK) predicts a velocity dispersion profile that is a continuously decreasing function of radius, in conflict with simulated profiles. We have extended the KLK approach to include radially varying  $\kappa$  distributions designed to more closely match the velocity behavior of simulation results. While this approach produces qualitative matches between the predictions and simulation results, there is no quantitative agreement. We describe four possible solutions to this problem.

1) Equations 1 and 2 correctly describe long-range collisionless gravitational interactions, but cosmological N-body simulations are not purely collisionless close to centers of halos due to numerical effects. In this case, a velocity dispersion that increases with radius (for  $r < r_0$ ) may indicate that artificial processes that mimic short-range interactions might be at play in the simulations. We do not speculate on what these might be (but see El-Zant 2005) or why they would lead to velocity dispersions increasing with radius. However, halos calculated from semi-analytical collapse models can reproduce both the density and velocity profiles of N-body halos, arguing against numerical effects.

2) The nonextensive approach of Equations 1 and 2 correctly predicts the global (asymptotic)

otic) equilibrium state, but N-body simulations (and possibly, real dark matter halos) settle to nonlocal or quasi-equilibria through instabilities, such as the radial orbit instability (Barnes *et al.* 2005).

3) Equations 1 and 2 do not correctly describe collisionless systems with long-range interactions, so a different thermodynamic approach needs to be found to describe dark matter halo simulations.

4) The approach taken in KLK and here does not account for velocity anisotropy which is present in halos formed in cosmological N-body simulations (Cole & Lacey 1996; Huss *et al.* 1999; Barnes *et al.* 2005; Hansen & Moore 2006; Hansen & Stadel 2006). Preliminary work by the authors that incorporates anisotropy into the nonextensive framework suggests that this is not a panacea. This adds to the evidence presented in Hansen *et al.* (2006) that suggests the presence of anisotropy in N-body halos requires that the distribution function have a more complex form than that given by Equation 3, pointing strongly towards the idea that a different thermodynamic approach must be taken for these systems (point 3 above).

Regardless of the validity of these points, further investigation of the relationship between nonextensive thermodynamics and self-gravitating systems is vital to providing a physical understanding, and independent corroboration, of the results of dark matter halo formation simulations.

This work has been supported by NSF grant AST-0307604. We thank Thomas Kronberger, Manfred Leubner, and Eelco van Kampen for thoughtful comments. We are also grateful to an anonymous referee who made several helpful suggestions. Research support for AB comes from the Natural Sciences and Engineering Research Council (Canada) through the Discovery grant program. AB would also like to acknowledge support from the Leverhulme Trust (UK) in the form of the Leverhulme Visiting Professorship at the Universities of Oxford and Durham. JJD was partially supported through the Alfred P. Sloan Foundation.

## REFERENCES

- Aly, J. J. 1993, in N-body Problems and Gravitational Dynamics, Proceedings of a meeting held at Centre Paul Langevin-CNRS Aussois, Haute Maurienne, France, 21-25 March 1993, eds., F. Combes and E. Athanassoula (Meudon: Observatoire de Paris), 19
- Austin, C. G., Williams, L. L. R., Barnes, E. I., Babul, A., Dalcanton, J. J. 2005, ApJ, 634, 756



- Barnes, E. I., Williams, L. L. R., Babul, A., Dalcanton, J. J. 2005, *ApJ*, 634, 775
- Cole, S., Lacey, C. 1996, *MNRAS*, 281, 716
- El-Zant, A. 2005, *astro-ph/0506617*
- Hansen, S. H., Egli, D., Hollenstein, L., Salzmann, C. 2005, *New A*, 10, 379
- Hansen, S. H., Moore, B. 2006, *New Astronomy*, 11, 333
- Hansen, S. H., Moore, B., Zemp, M., Stadel, J. 2006, *J. Cosmology Astropart. Phys.*, 01, 014
- Hansen, S. H., Stadel, J. 2006, *J. Cosmology Astropart. Phys.*, 05, 014
- Hoefl, M., Mücke, J.P., Gottlöber, S. 2004, *ApJ*, 602, 162
- Huss, A., Jain, B., Steinmetz, M. 1999, *ApJ*, 517, 64
- Kronberger, T., Leubner, M.P., van Kampen, E. 2006, *astro-ph/0603602*
- Leubner, M. P. 2005, *ApJ*, 632L, 1
- Lokas, E. L., 2000, *MNRAS*, 311, 423
- Lu, Y., Mo, H. J., Katz, N., Weinberg, M. D. 2006, *MNRAS*, 401
- Moore, B., Governato, F., Quinn, T., Stadel, J., Lake, G. 1998, *ApJ*, 499, L5
- Navarro, J. F., Frenk, C. S., White, S. D. M. 1996, *ApJ*, 462, 563
- Navarro, J. F., Hayashi, E., Power, C., Jenkins, A. R., Frenk, C. S., White, S. D. M., Springel, V., Stadel, J., Quinn, T. R. 2004, *MNRAS*, 349, 1039
- Nusser, A., 2001, *MNRAS*, 325, 1397
- Plastino, A. R., Plastino, A. 1993, *Phys. Lett. A*, 174, 384
- Power, C., Navarro, J. F., Jenkins, A., Frenk, C. S., White, S. D. M., Springel, V., Stadel, J., Quinn, T. 2003, *MNRAS*, 338, 14
- Silva, R., Plastino, A. R., Lima, J. A. S. 1998, *Phys. Lett. A*, 249, 401
- Taylor, J. E., Navarro, J. F. 2001, *ApJ*, 563, 483
- Tsallis, C. 1988, *J. Stat. Phys.*, 52, 479

Tsallis, C. 1999, Braz. J. Phys., 29, 1

Williams, L. L. R., Babul, A., Dalcanton, J. J. 2004, ApJ, 604, 18

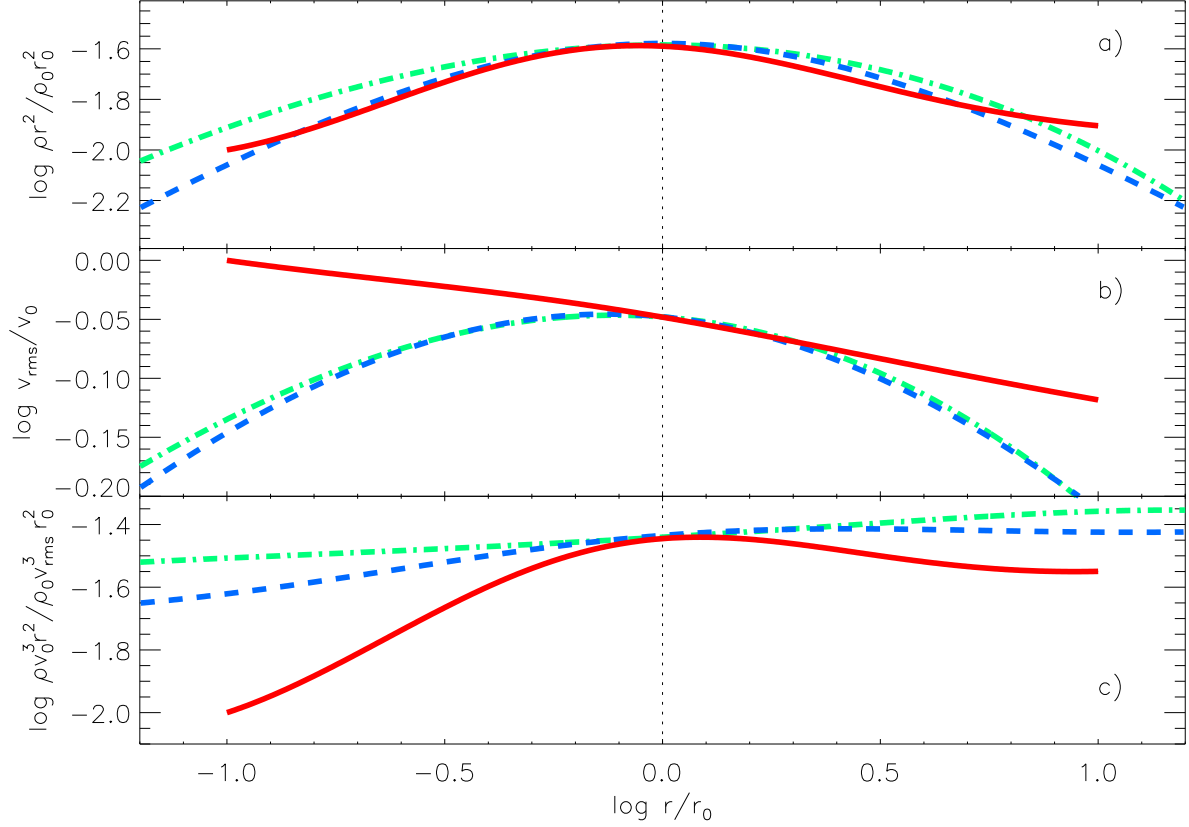


Fig. 1.— The constant  $\kappa$  nonextensive solutions for density (panel a), velocity dispersion (panel b), and  $\rho/v_{\text{rms}}^3$  (panel c) are given by the solid red lines. For comparison, corresponding curves for the NFW (dashed blue lines) and N04 (dash-dotted green lines) models are also shown. The density and  $\rho/v_{\text{rms}}^3$  profiles have been scaled by  $(r/r_0)^2$  to highlight variations from this power law distribution. The nonextensive  $v_{\text{rms}}$  distribution is monotonically decreasing, in stark contrast to the behavior of the simulation-based NFW and N04 models. This discrepancy is also evident when comparing the decidedly nonpower law shape of the solution  $\rho/v_{\text{rms}}^3$  profile to the very nearly power law empirical  $\rho/v_{\text{rms}}^3$  profiles. Note that the discrepancy is evident at radii that are well-resolved by simulations.

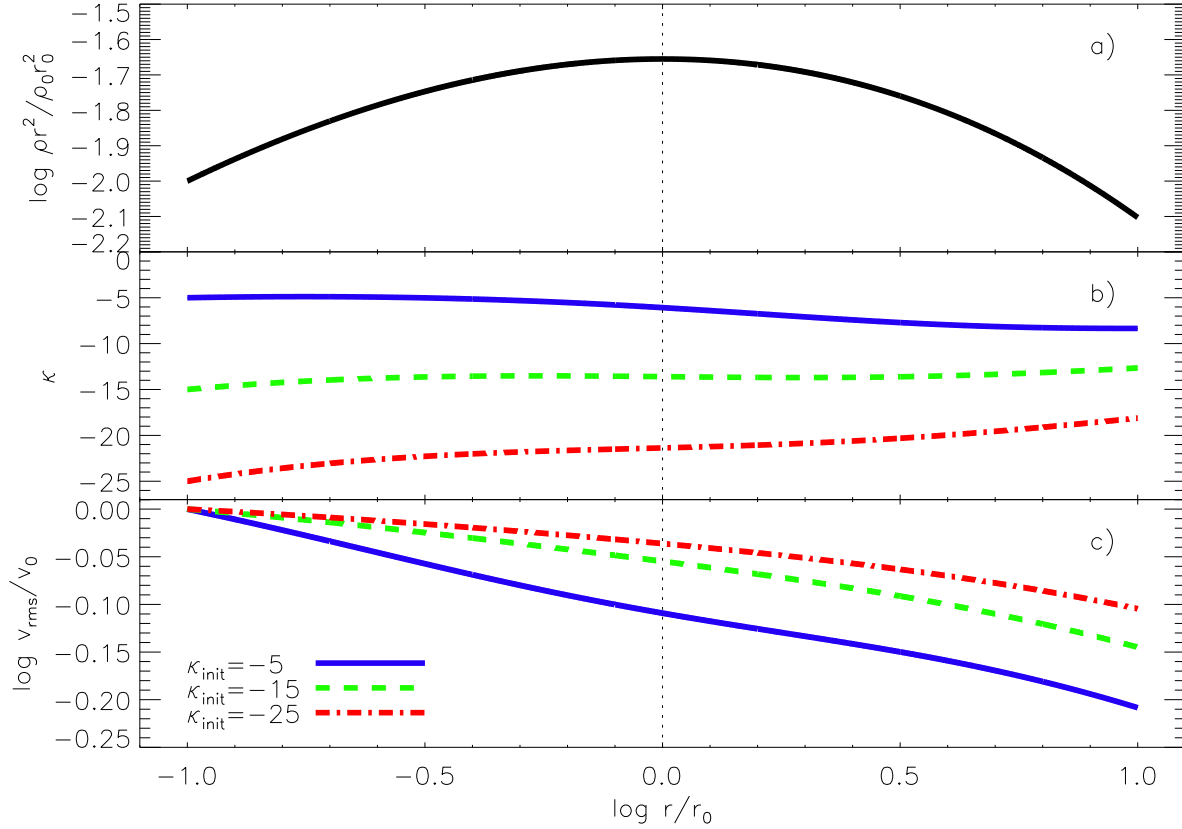


Fig. 2.— When  $\kappa$  is not constant, a  $\kappa$  profile can be found by solving Equation 6 with an assumed density distribution. The results shown here use the N04 density profile; adopting an NFW profile leads to very similar results. Panel a shows the scaled N04 density distribution that is shared by all of the solutions. The solution  $\kappa$  profiles (with  $\kappa_{\text{init}} = 0$ ) are shown in panel b. Here, the solid blue, dashed green, and dash-dotted red lines indicate solutions with  $\kappa_{\text{init}} = -5, -15$ , and  $-25$ , respectively. The velocity dispersion profiles (panel c) are monotonically decreasing, as in the constant  $\kappa$  case. Similarly, these  $v_{\text{rms}}$  profiles do not match those from simulations.

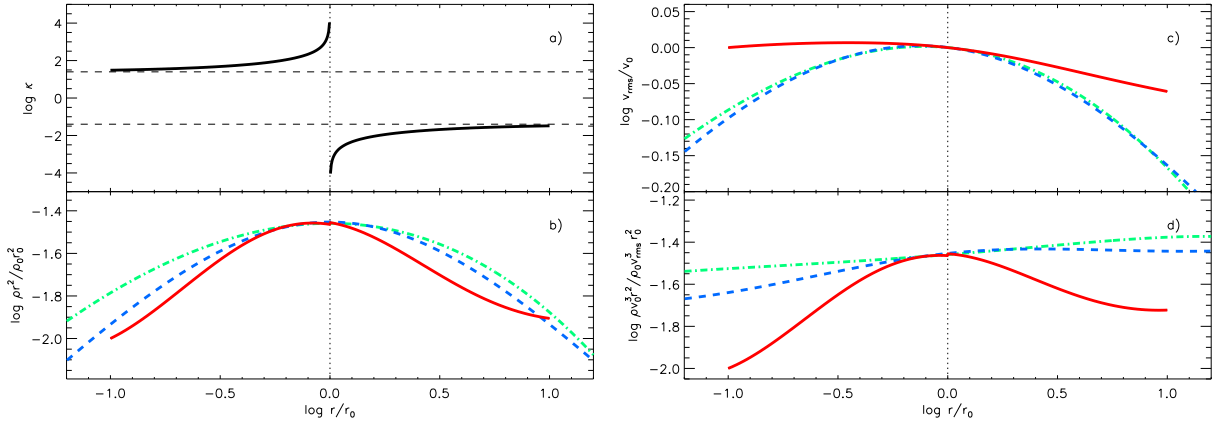


Fig. 3.— For the  $\kappa$  distribution described by Equation 7 (panel a), we show the nonextensive solutions (solid red lines) for density (panel b), velocity dispersion (panel c), and  $\rho/v_{\text{rms}}^3$  (panel d). For comparison, corresponding curves for the NFW (dashed blue lines) and N04 (dash-dotted green lines) models are also shown. As in Figure 1, the densities and  $\rho/v_{\text{rms}}^3$  profiles have been scaled by  $(r/r_0)^2$  to highlight variations. The solution curve is a decent match to the empirical density profiles in panel b. Close inspection of panel c reveals that the solution  $v_{\text{rms}}$  profile does first increase before decreasing, in qualitative agreement with the NFW and N04 curves. However, it is quantitatively very different from those curves, a fact also reflected in the discrepancies apparent in the  $\rho/v_{\text{rms}}^3$  profiles in panel d.